

# Information-Theoretical Approach to Relaxation Time Distribution in Rheology: Log-Normal Relaxation Spectrum Model

Takashi Uneyama

Department of Materials Physics, Graduate School of Engineering,  
Nagoya University,  
Furo-cho, Chikusa, Nagoya 464-8603, Japan

September 3, 2025

## Abstract

The relaxation modulus of a viscoelastic fluid can be decomposed into multiple Maxwell models and characterized by the relaxation spectrum for the relaxation time. It is empirically known that the logarithmic relaxation time is useful to express the relaxation spectrum. We use information geometry to analyze the relaxation modulus and shown that the logarithmic relaxation time is the most natural variable for the relaxation spectrum. Then we use information theory to estimate the most probable functional form for the relaxation spectrum. We show that the log-normal distribution is the information-theoretically most probable relaxation spectrum. We analyze the properties of the log-normal relaxation spectrum model and compare it with the fractional Maxwell model. The fractional Maxwell model with a small power-law exponent can be approximated as the log-normal relaxation spectrum model with a large standard deviation. We also compare the log-normal relaxation spectrum model with experimental linear viscoelasticity data for a high-density polyethylene, both at melt and solid states.

## 1 INTRODUCTION

The linear rheological behavior of a material can be characterized by the shear relaxation modulus  $G(t)$ , and the shear relaxation modulus can be expressed as[1]:

$$G(t) = \int_0^\infty d\tau \exp(-t/\tau)h(\tau), \quad (1)$$

where  $h(\tau)$  is the relaxation spectrum. Here we have assumed that the the material can flow at the long-time limit and thus  $G(t)$  decays exponentially at  $t \rightarrow \infty$ . Empirically, it is convenient to use the relaxation spectrum for the logarithmic relaxation time[1, 2]:

$$G(t) = \int_{-\infty}^\infty d(\ln \tau) \exp(-t/\tau)H(\ln \tau), \quad (2)$$

with  $H(\ln \tau) = \tau h(\tau)$ . Intuitively, we expect that  $H(\ln \tau)$  is preferred because it is expressed in the logarithmic scale: rheological properties are typically well described in the logarithmic scale than in the linear scale. Also, the relaxation time can be distributed in a very wide range, and the linear scale is not convenient. However, as far as the author knows, there is no *theoretical* support for the use of  $H(\ln \tau)$ . The first question considered in this work is whether we can theoretically explain that the use of  $H(\ln \tau)$  is most suitable or not.

When we use eq (1) or (2) to analyze rheological data, sometimes we need to employ some models for  $h(\tau)$  or  $H(\ln \tau)$ . For example, the Baumgaertel-Schausberger-Winter (BSW) spectrum model[3] may be used to analyze entangled polymer melts. If we have some microscopic or mesoscopic molecular models for target systems, we may be able to estimate the relaxation spectra starting from molecular models. However, if the information about target systems is very limited, we cannot employ molecular models for specific systems. Instead, we will require a general relaxation spectrum model which is applicable to various systems. The second question considered in this work is what is this general relaxation spectrum model.

To answer two questions raised above, in this work we conduct information-theoretical analyses for the relaxation modulus. We show that the relaxation spectrum for the logarithmic relaxation time  $H(\ln \tau)$  can be interpreted as the most natural form, from the viewpoint of information geometry[4, 5]. (The meaning of “natural” used here will be explained later.) We also show that the information-theoretically natural relaxation spectrum is the Gaussian distribution for the logarithmic relaxation time. It corresponds to the log-normal relaxation spectrum model[2]. We analyze the properties of the log-normal relaxation spectrum model in detail. In some aspects, the log-normal relaxation spectrum model has similar properties to the fractional Maxwell model[6, 2]. We compare two models and show the similarities and differences between them. Then we apply the log-normal relaxation spectrum model to experimental shear relaxation modulus data of a high-density polyethylene. The terminal relaxation behavior of an entangled polydisperse polymer melt can be reasonably reproduced by the log-normal relaxation spectrum model. The storage and loss moduli of a crystalline polymer solid can be also reproduced by the log-normal relaxation spectrum model.

## 2 THEORY

### 2.1 Information Geometry for Relaxation Spectrum

The relaxation modulus of the (single) Maxwell model with the relaxation time  $\tau$  and the relaxation intensity (or the limiting modulus)  $g$  is expressed as

$$G_M(t|\tau) = g \exp(-t/\tau). \quad (3)$$

If we define the normalized relaxation modulus as  $\Phi_M(t|\tau) = G_M(t|\tau)/g = \exp(-t/\tau)$ , we have  $\Phi_M(0|\tau) = 1$  and  $\partial\Phi_M(t|\tau)/\partial t < 0$  ( $\Phi_M(t|\tau)$  is a monotonically decreasing function of  $t$ ). Therefore, we may interpret  $\Phi_M(t|\tau)$  as the survival function[7] of the stress. This interpretation can be also supported by a microscopic molecular model. According to the linear response theory[8], the relaxation modulus can be related to the auto-correlation function of the stress fluctuation. If we normalize the relaxation modulus, it becomes the normalized correlation function which may be interpreted as the survival function. By taking the derivative of the survival function, we have the probability density:

$$P_M(t|\tau) = -\frac{\partial\Phi_M(t|\tau)}{\partial t} = \frac{1}{\tau} \exp(-t/\tau). \quad (4)$$

Eq (4) can be interpreted as the probability density for the “life time” of the stress.

In general, the relaxation modulus is expressed as the superposition of Maxwell models with various relaxation times (the generalized Maxwell model), as eq (1). Then the probability density for the life time becomes

$$P(t) = -\frac{1}{G_0} \frac{\partial G(t)}{\partial t} = \int_0^\infty d\tau P_M(t|\tau) \tilde{h}(\tau), \quad (5)$$

with the total relaxation intensity  $G_0$  and the normalized relaxation spectrum  $\tilde{h}(\tau)$  defined as

$$G_0 = G(0) = \int_0^\infty d\tau h(\tau), \quad (6)$$

$$\tilde{h}(\tau) = \frac{1}{G_0} h(\tau). \quad (7)$$

$\tilde{h}(\tau)$  is normalized and thus it can be interpreted as the probability density for the relaxation time  $\tau$ . Eq (5) may be interpreted as the combination of two probability densities,  $P_M(t|\tau)$  and  $\tilde{h}(\tau)$ , and such a combination is sometimes called superstatistics[9].

If we introduce a (nonlinear) variable transform from  $\tau$  to  $\xi$ , we will have the probability density  $P(t)$  expressed in terms of the probability density for  $\xi$ . Any variable transform gives the same probability density  $P(t)$ . But the superstatistical meaning depends on  $\xi$ . In general, the parameter space for  $\xi$  is not a Euclidean space but a Riemannian space, and the metric which characterizes it is not constant. We consider that the most “natural” variable transform is that gives constant metric.

Here we utilize the theory of information geometry[4, 5] to seek the natural variable transform. In information geometry, we can quantitatively measure the “distance” between different probability densities and analyze the geometrical properties for probability densities. They will be useful to select the natural variable transform among various candidates.

We consider two Maxwell models with different relaxation times. The distance between two probability densities with different relaxation times can be calculated based on the probability density (4). We assume that two relaxation times for two probability densities are sufficiently close:  $\tau$  and  $\tau + d\tau$  ( $d\tau$  is assumed to be sufficiently small). According to information geometry[4, 5], the distance between these probability densities,  $dL$ , is given as

$$dL^2 = I(\tau)d\tau^2, \quad (8)$$

where  $I(\tau)$  is the Fisher information defined as:

$$I(\tau) = \int_0^\infty dt P_M(t|\tau) \left[ \frac{\partial \ln P_M(t|\tau)}{\partial \tau} \right]^2 = \frac{1}{\tau^2}. \quad (9)$$

Intuitively, the Fisher information (9) characterizes the degree of change of  $P_M(t|\tau)$  to the change of its parameter  $\tau$ . (The Fisher information was originally introduced for an optimization problem[10], but currently it is also utilized in several different fields such as information geometry.) By combining eqs (8) and (9), we have the distance between two probability densities with relaxation times  $\tau'$  and  $\tau''$ :

$$L(\tau'', \tau') = \int_{\tau'}^{\tau''} dL = \int_{\tau'}^{\tau''} \sqrt{\frac{1}{\tau^2}} d\tau = |\ln \tau' - \ln \tau''|. \quad (10)$$

Eq (10) means that the distance between two probability densities with  $\tau'$  and  $\tau''$  is *not*  $|\tau' - \tau''|$  (which corresponds to the simple Euclidean distance). This is not surprising because the information geometry states that the space for a family of probability densities generally becomes a Riemannian space. The Fisher information  $I(\tau)$  in eq (8) can be interpreted as the metric in the Riemannian geometry[11]. By using a variable transform, a one-dimensional Riemannian space can be transformed into a one-dimensional Euclidean space. (This is because the Riemann curvature is trivially zero in a one-dimensional space[11].) We employ  $\xi = \ln(\tau/\tau_0)$  instead of  $\tau$ . Here,  $\tau_0$  is a characteristic relaxation time of the target system. The distance between  $\xi' = \ln(\tau'/\tau_0)$  and  $\xi'' = \ln(\tau''/\tau_0)$  simply becomes  $L(\xi'', \xi') = |\xi' - \xi''|$ , which is the Euclidean distance. The Fisher information for  $\xi$  becomes unity, as expected:

$$I'(\xi) = \int_0^\infty dt P_M(t|\tau_0 e^\xi) \left[ \frac{\partial \ln P_M(t|\tau_0 e^\xi)}{\partial \xi} \right]^2 = 1. \quad (11)$$

With this new variable, we have

$$P(t) = \int_{-\infty}^\infty d\xi P_M(t|\tau_0 e^\xi) \tilde{H}(\xi), \quad (12)$$

where

$$\tilde{H}(\xi) = \tau_0 e^\xi \tilde{h}(\tau_0 e^\xi) \quad (13)$$

is the normalized relaxation spectrum.  $\tilde{H}(\xi)$  can be interpreted as the probability density for  $\xi$ .

From the viewpoint of information geometry,  $\xi = \ln(\tau/\tau_0)$  is the most “natural” parameter which characterizes the probability density (4). Therefore, the information-theoretically most natural expression for the relaxation modulus  $G(t)$  is

$$G(t) = \int_{-\infty}^{\infty} d\xi \exp(-t/\tau_0 e^{-\xi}) H(\xi), \quad (14)$$

with

$$H(\xi) = G_0 \tilde{H}(\xi) = \tau_0 e^{\xi} h(\tau_0 e^{\xi}). \quad (15)$$

Eq (14) coincides with eq (2) if we set  $\tau_0 = 1$ . ( $\tau_0$  is the characteristic relaxation time and can be taken rather arbitrarily.) We conclude that the relaxation spectrum for the logarithmic relaxation time,  $H(\xi)$ , is *the most natural and suitable expression*, from the view point of information geometry. This is the answer to the first question.

## 2.2 Most Probable Distribution for Relaxation Time

If  $\xi = \ln(\tau/\tau_0)$  is used instead of  $\tau$ , we can treat the space for the family of  $P_M(t|\tau_0 e^{\xi})$  as just the one dimensional Euclidean space. We use this property to determine the most probable functional form for the relaxation spectrum. As we mentioned,  $\tilde{H}(\xi)$  is normalized and thus can be interpreted as the probability density for  $\xi$ .

In this subsection, we derive the information-theoretically most probable probability density for  $\xi$ . According to information theory, the most probable probability density is given as the probability density which maximizes the Shannon entropy. The Shannon entropy is given as a functional of the probability density  $\tilde{H}(\xi)$ [12]:

$$\mathcal{S}[\tilde{H}] = - \int_{-\infty}^{\infty} d\xi \tilde{H}(\xi) \ln \tilde{H}(\xi). \quad (16)$$

Here, we should stress that the Shannon entropy is well-defined only in the Euclidean space. Thus we should *not* utilize  $\tau$  and  $\tilde{h}(\tau)$  instead of  $\xi$  and  $\tilde{H}(\xi)$ .

The probability density which maximizes eq (16) under some constraints can be interpreted as the information-theoretically most probable distribution. Since  $\tilde{H}(\xi)$  can be interpreted as the probability density, it should be normalized and we need to introduce the following constraint:

$$\int_{-\infty}^{\infty} d\xi \tilde{H}(\xi) = 1. \quad (17)$$

In addition, some moments of  $\xi$  need to be constrained. The first moment of  $\xi$  is the mean, but we do not need to constrain it. We have already introduced the characteristic relaxation time  $\tau_0$  and it can be used to control the mean value of  $\ln \tau$ . The second moment of  $\xi$  is the variance (or the squared standard deviation). Thus we employ the following constraint:

$$\int_{-\infty}^{\infty} d\xi \xi^2 \tilde{H}(\xi) = s^2, \quad (18)$$

where  $s \geq 0$  is the standard deviation of  $\xi$ . We maximize the Shannon entropy (16) with respect to  $\tilde{H}(\xi)$  under the constraints (17) and (18). The maximization can be easily done by using the Lagrange multiplier method. That is, we maximize

$$\mathcal{S}'[\tilde{H}] = \mathcal{S}[\tilde{H}] + \lambda \int_{-\infty}^{\infty} d\xi \tilde{H}(\xi) + \mu \int_{-\infty}^{\infty} d\xi \xi^2 \tilde{H}(\xi), \quad (19)$$

instead of  $\mathcal{S}[\tilde{H}]$ . Here,  $\lambda$  and  $\mu$  are Lagrange multipliers and they will be determined afterward, so that the constraints (17) and (18) are satisfied. The maximization of eq (19) gives

$$0 = \frac{\delta \mathcal{S}'[\tilde{H}]}{\delta \tilde{H}(\xi)} = 1 + \ln \tilde{H}(\xi) + \lambda + \mu \xi^2. \quad (20)$$

In eq (20),  $\delta/\delta\tilde{H}(\xi)$  represents the functional differential. The solution of eq (20) is the normal distribution:

$$\tilde{H}(\xi) = \frac{1}{\sqrt{2\pi s^2}} \exp\left(-\frac{\xi^2}{2s^2}\right), \quad (21)$$

where we have determined the Lagrange multipliers as  $\lambda = -1 + (1/2)\ln(2\pi s^2)$  and  $\mu = 1/2\sigma^2$  from constraints (17) and (18), and substituted them into the expression of  $\tilde{H}(\xi)$ .

Eq (21) is the information-theoretically most probable relaxation spectrum under the constraints (17) and (18). If we introduce some additional constraints, we have different most probable relaxation spectra. But the number of parameters increase as we increase the number of constraints. A model with the smallest number of constraints will be convenient. If we remove the constraint for the standard deviation, eq (18), the resulting distribution will be that with the smaller number of parameters. However, this is not possible. Without the constraint for the standard deviation, the maximization condition becomes  $0 = 1 + \ln \tilde{H}(\xi) + \lambda$  instead of eq (20). This gives the constant probability density:  $\tilde{H}(\xi) = (\text{const.})$ . But  $\xi$  is defined in the range  $-\infty < \xi < \infty$  and the constant probability density cannot be realized. Thus we conclude that the normal distribution (21) is the most probable functional form with the smallest number of parameters.

The unnormalized relaxation spectra  $H(\xi)$  and  $h(\tau)$  which correspond to eq (21) become

$$H(\xi) = \frac{G_0}{\sqrt{2\pi s^2}} \exp\left(-\frac{\xi^2}{2s^2}\right), \quad (22)$$

$$h(\tau) = \frac{G_0}{\sqrt{2\pi s^2}\tau} \exp\left[-\frac{(\ln \tau - \ln \tau_0)^2}{2s^2}\right]. \quad (23)$$

Eq (23) is the log-normal probability density. Therefore, we call the linear viscoelasticity model with eq (22) or eq (23) as the log-normal relaxation spectrum model[2]. The answer to the second question is that we can use the log-normal relaxation spectrum model if the information about the target systems is very limited. It is the *information-theoretically most probable* relaxation spectrum model. The log-normal relaxation spectrum model has three parameters: the total relaxation intensity  $G_0$ , the characteristic relaxation time  $\tau_0$ , and the standard deviation  $s$ .  $G_0$  and  $\tau_0$  simply determine the stress and time scales, and the shape of the relaxation modulus depends only on  $s$ .

### 2.3 Properties of Log-Normal Relaxation Spectrum Model

Although the use of the log-normal relaxation spectrum model has been reported in literature[13, 14, 15], it is not that popular. Thus its properties are not well-known, compared with other empirical models. Here we study some properties of the log-normal relaxation time spectrum model. The relaxation modulus is given by substituting eq (22) into eq (14). The storage and loss moduli are calculated from the relaxation spectrum as

$$G'(\omega) = \int_{-\infty}^{\infty} d\xi \frac{(\tau_0 e^{\xi\omega})^2}{1 + (\tau_0 e^{\xi\omega})^2} H(\xi), \quad (24)$$

$$G''(\omega) = \int_{-\infty}^{\infty} d\xi \frac{\tau_0 e^{\xi\omega}}{1 + (\tau_0 e^{\xi\omega})^2} H(\xi), \quad (25)$$

with  $H(\xi)$  by eq (22). At the limit of  $s \rightarrow 0$ ,  $H(\xi)$  approaches to the Dirac delta function:  $H(\xi) \rightarrow G_0\delta(\xi)$ . Thus the log-normal relaxation model reduces to the Maxwell model at  $s = 0$ .

We numerically calculate  $G(t)$ ,  $G'(\omega)$ , and  $G''(\omega)$  of the log-normal relaxation spectrum model. The double exponential formula is used to perform the numerical integration method[16, 17]. Fig. 1 shows numerically calculated  $G(t)$ ,  $G'(\omega)$ , and  $G''(\omega)$  for  $s = 2.5, 5, 7.5$ , and 10. For comparison, the data for  $s = 0$  (which corresponds to the Maxwell model) are also shown. As  $s$  increases, we observe that moduli become broad.  $G(t)$  with  $s = 10$  do not decay exponentially at least in the plotted range ( $t/\tau_0 \leq 10^6$ ). Also, we cannot observe the terminal region for  $G'(\omega)$  and  $G''(\omega)$  with  $s = 10$  in the plotted range ( $\tau_0\omega \geq 10^{-6}$ ). However, the log-normal relaxation model exhibits the terminal behavior at the sufficiently low frequency region for any  $s$ , as we will show. The loss

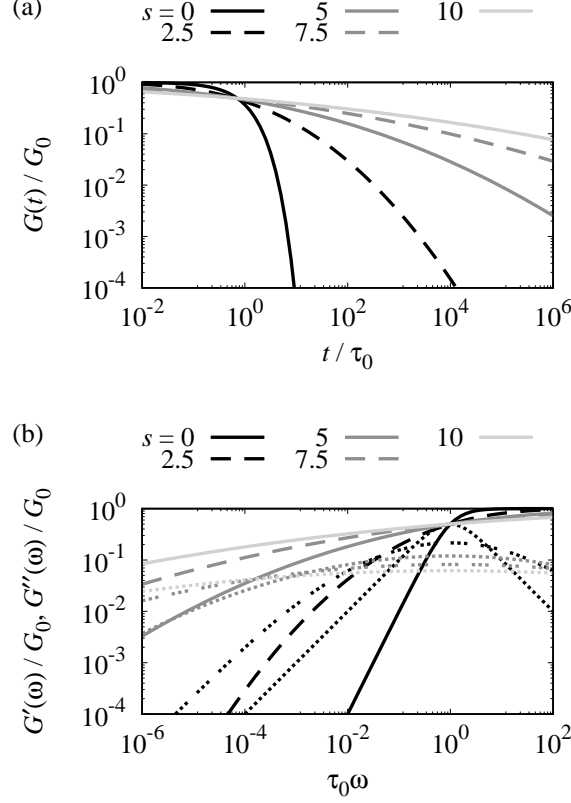


Figure 1: (a) Relaxation moduli  $G(t)$  and (b) storage and loss moduli  $G'(\omega)$  and  $G''(\omega)$  of the log-normal relaxation spectrum model with  $s = 0, 2.5, 5, 7.5$ , and  $10$ . In (b), solid and dashed curves indicate  $G'(\omega)$  whereas dotted and dot-dashed curves indicate  $G''(\omega)$ . In the case of  $s = 0$ , the log-normal relaxation spectrum model reduces to the Maxwell model.

modulus  $G''(\omega)$  in Fig. 1(b) seems symmetric around its peak at  $\tau_0\omega = 1$ . This symmetry can be derived straightforwardly. From eq (22),  $H(\xi)$  is symmetric:  $H(\xi) = H(-\xi)$ . If we introduce a variable transform  $\xi' = -\xi$ , eq (25) gives

$$\begin{aligned}
 G''(\omega) &= \int_{-\infty}^{\infty} d\xi' \frac{\tau_0 e^{-\xi'\omega}}{1 + (\tau_0 e^{-\xi'\omega})^2} H(-\xi') \\
 &= \int_{-\infty}^{\infty} d\xi' \frac{\tau_0 e^{\xi'} (\tau_0^{-2}\omega^{-1})}{1 + [\tau_0 e^{\xi'} (\tau_0^{-2}\omega^{-1})]^2} H(\xi') \\
 &= G''(\tau_0^{-2}\omega^{-1}).
 \end{aligned} \tag{26}$$

The average of  $\tau^p$  (with  $p$  being an integer) is calculated as

$$\langle \tau^p \rangle = \int_{-\infty}^{\infty} d\xi (\tau_0 e^{\xi})^p \tilde{H}(\xi) = \tau_0^p \exp(p^2 s^2 / 2). \tag{27}$$

Then we have the following first- and second-moment average relaxation times:

$$\langle \tau \rangle_n = \langle \tau \rangle = \tau_0 \exp(s^2 / 2), \tag{28}$$

$$\langle \tau \rangle_w = \langle \tau^2 \rangle / \langle \tau \rangle = \tau_0 \exp(3s^2 / 2). \tag{29}$$

Thus both  $\langle \tau \rangle_n$  and  $\langle \tau \rangle_w$  are finite. This is in contrast to some empirical models such as the fractional Maxwell model[6, 2]. Fig. 2 shows  $\langle \tau \rangle_n$  and  $\langle \tau \rangle_w$  by eqs (28) and (29). We can observe

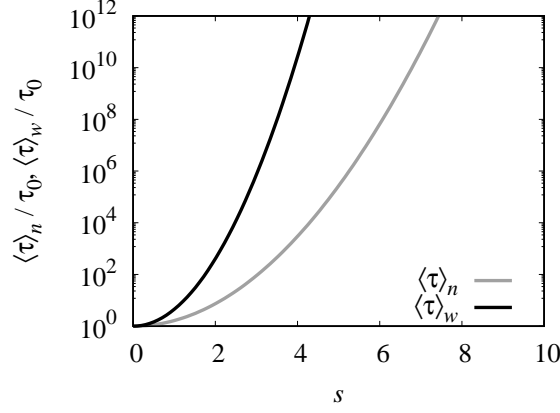


Figure 2: First- and second-moment average relaxation times  $\langle \tau \rangle_n$  and  $\langle \tau \rangle_w$  for the log-normal relaxation spectrum model.

that both relaxation times increase rapidly as  $s$  increases. If  $s$  is relatively large, practically we will not be able to observe the relaxation.

Eqs (28) and (29) mean that the terminal behaviors are observed for the storage and loss moduli at the low-frequency region. For  $\tau_0\omega \ll 1$ , we have

$$G'(\omega) \approx G_0 \langle \tau^2 \rangle \omega^2 = G_0 \tau_0^2 \exp(2s^2) \omega^2, \quad (30)$$

$$G''(\omega) \approx G_0 \langle \tau \rangle \omega = G_0 \tau_0 \exp(s^2/2) \omega. \quad (31)$$

From eq (31), the zero-shear viscosity is

$$\eta_0 = G_0 \tau_0 \exp(s^2/2). \quad (32)$$

For  $\tau_0\omega \gg 1$ , we have

$$G'(\omega) \approx G_0, \quad (33)$$

$$G''(\omega) \approx \frac{G_0 \langle \tau \rangle}{\tau_0^2 \omega} = \frac{G_0 \exp(s^2/2)}{\tau_0 \omega}. \quad (34)$$

Here, we have utilized eqs (26) and (31) to derive eq (34).

## 3 DISCUSSIONS

### 3.1 Comparison with Fractional Maxwell Model

One interesting property of the log-normal relaxation spectrum model is that  $\tilde{H}(\xi)$  is symmetric:  $\tilde{H}(\xi) = \tilde{H}(-\xi)$ . In this section we compare the log-normal relaxation spectrum model with the fractional Maxwell model[6, 2], of which  $\tilde{H}(\xi)$  has the same symmetry. The fractional Maxwell model is often related to the fractional derivative model[6, 18], and it is equivalent to the Cole-Cole model for dielectric relaxation[19, 20, 18].

The fractional Maxwell model can be defined as a simple form in the frequency domain. The storage and loss moduli are given as

$$G'(\omega) + iG''(\omega) = G_0 \frac{(i\tau_0\omega)^\alpha}{1 + (i\tau_0\omega)^\alpha}, \quad (35)$$

where  $G_0$  is the total relaxation intensity,  $\tau_0$  is the characteristic relaxation time, and  $0 < \alpha \leq 1$  is the exponent. (For  $\alpha = 1$ , eq (35) reduces to the Maxwell model (3).) Eq (35) can be rewritten

as follows:

$$G'(\omega) = G_0 \frac{(\tau_0 \omega)^{2\alpha} + \cos(\alpha\pi/2) (\tau_0 \omega)^\alpha}{[(\tau_0 \omega)^\alpha + \cos(\alpha\pi/2)]^2 + \sin^2(\alpha\pi/2)}, \quad (36)$$

$$G''(\omega) = G_0 \frac{\sin(\alpha\pi/2) (\tau_0 \omega)^\alpha}{[(\tau_0 \omega)^\alpha + \cos(\alpha\pi/2)]^2 + \sin^2(\alpha\pi/2)}. \quad (37)$$

The fractional Maxwell model does not exhibit the terminal behavior. For  $\tau_0 \omega \ll 1$ , we have

$$G'(\omega) \approx G_0 \cos(\alpha\pi/2) (\tau_0 \omega)^\alpha, \quad (38)$$

$$G''(\omega) \approx G_0 \sin(\alpha\pi/2) (\tau_0 \omega)^\alpha. \quad (39)$$

Thus the fractional Maxwell model behaves in the same way as the critical gel[21]:  $G'(\omega) \propto G''(\omega) \propto \omega^\alpha$  and  $\tan \delta(\omega) = \tan(\alpha\pi/2)$ . This means that the fractional Maxwell model does not flow. (The same critical-gel behavior is observed for the Havriliak-Negami model[22].) The first- and second-moment average relaxation times and the zero-shear viscosity diverge. This is in contrast to the log-normal relaxation spectrum model.

In the time domain, the relaxation modulus  $G(t)$  of the fractional Maxwell model cannot be expressed in terms of the elementary functions.  $G(t)$  is expressed as

$$G(t) = G_0 E_\alpha[-(t/\tau_0)^\alpha], \quad (40)$$

where  $E_\alpha(x)$  is the Mittag-Leffler function[6, 23]. For  $0 < \alpha < 1$  and  $t \gg \tau_0$ , eq (40) can be approximated as

$$G(t) \approx G_0 \frac{(t/\tau_0)^\alpha}{\Gamma(1-\alpha)}, \quad (41)$$

where  $\Gamma(x)$  is the gamma function[24]. Thus the fractional Maxwell model exhibits the power-law tail:  $G(t) \propto t^{-\alpha}$ . This is consistent with the lack of the terminal behavior in the storage and loss moduli.

Fig. 3 shows  $G(t)$ ,  $G'(\omega)$ , and  $G''(\omega)$  of the fractional Maxwell model with  $\alpha = 0.2, 0.4, 0.6, 0.8$ , and 1. Here, the Mittag-Leffler function is numerically calculated[25]. We observe the power-law tail (eq (41)) at the long-time region in Fig. 3(a), and the critical-gel behavior (eqs (38) and (39)) at the low-frequency region in Fig. 3(b), except the case of  $\alpha = 1$ . The loss modulus data in Fig. 3 seem to have the symmetry  $G''(\omega) = G''(\tau_0^{-2}\omega^{-1})$ , which is the same property as the log-normal relaxation spectrum model. If we compare the data in Figs. 1 and 3, we observe that the fractional Maxwell model with relatively small  $\alpha$  (such as  $\alpha = 0.2$ ) exhibits similar trends to the log-normal relaxation spectrum model with large  $s$ .

Although eq (40) is not simple, the corresponding relaxation spectrum can be expressed in terms of the elementary functions[6, 26]:

$$H(\xi) = \frac{G_0}{2\pi} \frac{\sin(\alpha\pi)}{\cosh(\alpha\xi) + \cos(\alpha\pi)}. \quad (42)$$

Fig. 4 shows the relaxation spectrum by eq (42). We observe that  $H(\xi)$  of the fractional Maxwell model has a single peak at  $\xi = 0$  and is symmetric:  $H(\xi) = H(-\xi)$ . (This symmetry gives  $G''(\omega) = G''(\tau_0^{-2}\omega^{-1})$ .)

For relatively small  $\alpha$ , the peak shape of  $H(\xi)$  in Fig. 4 seems to be similar to that of the Gaussian. Thus we expect that  $H(\xi)$  of the fractional Maxwell model can be approximated by that of the log-normal relaxation spectrum model. We expand eq (42) around  $\xi = 0$  and approximate  $H(\xi)$  as

$$\ln H(\xi) \approx \ln \left[ \frac{G_0}{2\pi} \frac{\sin(\alpha\pi)}{1 + \cos(\alpha\pi)} \right] - \frac{\alpha^2}{2[1 + \cos(\alpha\pi)]} \xi^2. \quad (43)$$

By comparing eq (43) with eq (22), we find that the fractional Maxwell model can be approximated as the log-normal relaxation spectrum model:

$$H(\xi) \approx \frac{G_{0,\text{eff}}}{\sqrt{2\pi s_{\text{eff}}^2}} \exp \left( -\frac{\xi^2}{2s_{\text{eff}}^2} \right), \quad (44)$$

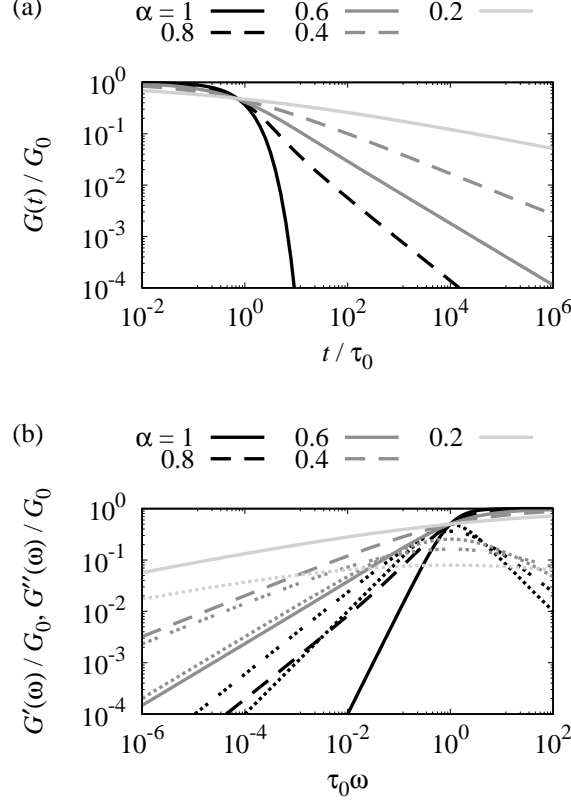


Figure 3: (a) Relaxation moduli  $G(t)$  and (b) storage and loss moduli  $G'(\omega)$  and  $G''(\omega)$  of the fractional Maxwell model with  $\alpha = 0.2, 0.4, 0.6, 0.8$ , and  $1$ .  $\alpha = 1$  corresponds to the Maxwell model.

where  $G_{0,\text{eff}}$  and  $s_{\text{eff}}$  are given as

$$G_{0,\text{eff}} = \frac{G_0}{\sqrt{2\pi}} \frac{\sin(\alpha\pi)}{\alpha\sqrt{1+\cos(\alpha\pi)}}, \quad (45)$$

$$s_{\text{eff}} = \frac{\sqrt{1+\cos(\alpha\pi)}}{\alpha}. \quad (46)$$

From eq (46),  $s_{\text{eff}} = 0$  for  $\alpha = 1$ . Thus the Maxwell model is correctly recovered, as expected. Also, at the limit of  $\alpha \rightarrow 0$ ,  $s_{\text{eff}}$  diverges ( $s_{\text{eff}} \rightarrow \infty$ ).

By using eq (46), we can estimate the standard deviation of the log-normal relaxation model from the exponent of the fractional Maxwell model. Of course, the fractional Maxwell model does not coincide to the log-normal relaxation model. The correspondence between two models is justified only in the limited time or frequency range. As an example, we show storage and loss moduli of the fractional Maxwell model and those of the log-normal relaxation spectrum model with parameters  $s_{\text{eff}}$  and  $G_{0,\text{eff}}$  estimated by eqs (45) and (46), in Fig. 5. We observe that the loss moduli of two models agree very well around  $\tau_0\omega = 1$ . The log-normal relaxation model may be used as an approximation for the fractional Maxwell model around the peak of the loss modulus, and vice versa.

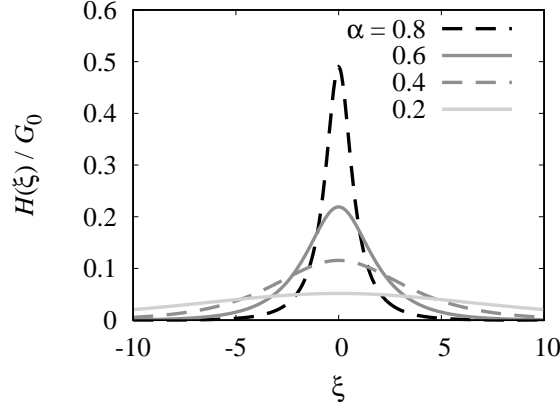


Figure 4: Relaxation spectra of the fractional Maxwell model with  $\alpha = 0.2, 0.4, 0.6, 0.8$ . (For  $\alpha = 1$ , the relaxation spectra becomes the Dirac delta function and thus not shown here.)

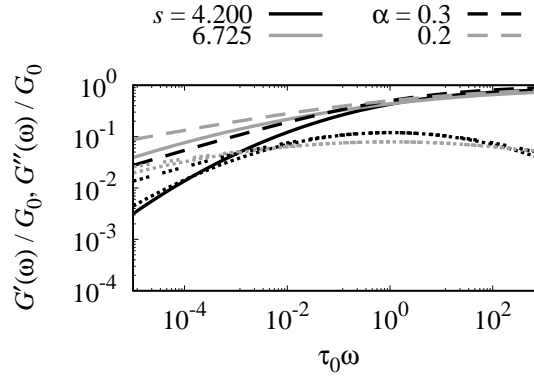


Figure 5: Comparison of the storage and loss moduli of the fractional Maxwell model (solid and dotted curves) and the log-normal relaxation spectrum model (dashed and dot-dashed curves).  $\alpha = 0.2$  and  $0.3$  for the fractional Maxwell model, and  $s$  and  $G_0$  for the log-normal relaxation spectrum model are calculated by eqs (45) and (46).

### 3.2 Comparison with Experimental Data

In this subsection, we attempt to utilize the log-normal relaxation spectrum model to analyze some experimental rheology data. Here we employ storage and loss moduli data of high-density polyethylene (HDPE, Sigma-Aldrich, 547999) in melt and solid states. The details of the experiments are summarized in Appendix A.

The molecular weight distribution of a commercial HDPE is typically broad. As a result, often we cannot observe the clear terminal behavior at the low-frequency region. Fulchiron and coworkers[13] reported that the storage and loss moduli of some commercial polypropylenes can be fitted to the log-normal relaxation spectrum model[13]. We expect that the storage and loss moduli of an HDPE melt can be also expressed well as the log-normal relaxation spectrum model.

Fig. 6 shows the storage and loss moduli of an HDPE melt, and those by the log-normal relaxation spectrum model. The experimental data are master curves constructed with the data at several different temperatures by the time-temperature superposition. The reference temperature for the master curves is  $T_{\text{ref}} = 140^\circ\text{C}$ . The parameters in the log-normal relaxation spectrum model are tuned manually. The results are  $G_0 = 1.1 \times 10^6$  Pa,  $\tau_0 = 6.5 \times 10^{-5}$  s, and  $s = 3.4$ .

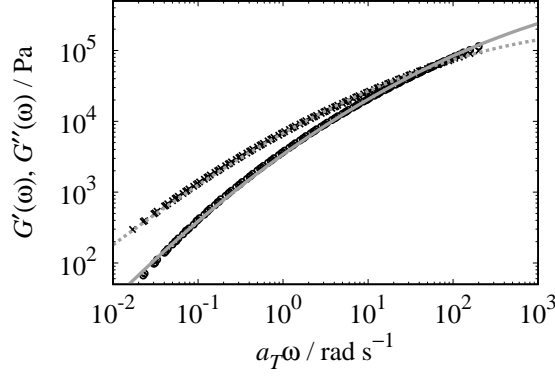


Figure 6: Storage and loss moduli of an HDPE melt at the reference temperature  $T_{\text{ref}} = 140^\circ\text{C}$  (circles and crosses) and the log-normal relaxation spectrum model (solid and dotted curves). The parameters for the log-normal relaxation spectrum model are  $G_0 = 1.1 \times 10^6 \text{ Pa}$ ,  $\tau_0 = 6.5 \times 10^{-5} \text{ s}$ , and  $s = 3.4$ .

Although the agreement is not perfect, we observe that the broad relaxation mode distribution is well captured by the log-normal relaxation model. By using eq (29), the second-moment average relaxation time is estimated as  $\langle \tau \rangle_w = 2.2 \times 10^3 \text{ s}$ . Considering the fact that the terminal behavior is not observed in Fig. 6, this estimate seems to be reasonable.

HDPE is a typical crystalline polymer and form crystalline structures when cooled and solidified from a melt. Crystalline polymer solids exhibit very broad relaxation time distributions[27], which reflect motions of polymer chains in crystalline lamellar superstructures. It is not easy to characterize their rheological behaviors from the frequency-dependence of the storage and loss moduli.

Fig. 7 shows the storage and loss moduli of an HDPE solid, and the those by the log-normal relaxation spectrum model. The experimental data are master curves constructed by the time-temperature superposition, and the reference temperature is  $T_{\text{ref}} = 100^\circ\text{C}$ . Both the storage and loss moduli weakly depend on the frequency, and we cannot observe the terminal behavior in the examined angular frequency range. As before, the parameters in the log-normal relaxation spectrum model are tuned manually, and we have  $G_0 = 1.2 \times 10^8$ ,  $\tau_0 = 1.0 \times 10^{-3}$ , and  $s = 9.0$ . The value of  $s$  is much larger than that for a melt. (Because  $s$  is large, the fractional Maxwell model may be utilized as well. From eq (46), the exponent of the corresponding fractional Maxwell model will be  $\alpha = 0.15$ .) Although the log-normal relaxation spectrum model does not perfectly reproduce the experimental data, it reasonably mimics a very broad relaxation time distribution. The second-moment average relaxation time can be estimated as  $\langle \tau \rangle_w = 5.8 \times 10^{49} \text{ s}$ . The relaxation time is extremely long and practically it is impossible to observe by experiments. This result is consistent with our naive expectation.

## 4 CONCLUSIONS

We analyzed the relaxation modulus by using information geometry and information theory. We showed that the distance between probability densities with different life times becomes the Euclidean distance, if we employ the logarithmic relaxation time  $\xi = \ln(\tau/\tau_0)$ . This result theoretically supports the use of  $H(\xi)$ , instead of  $h(\tau)$ , as the most natural and suitable expression. We also showed that the most probable distribution for  $\xi$  is the normal distribution, and thus the log-normal relaxation spectrum model is the information-theoretically most probable relaxation model. We analyzed the properties of the log-normal relaxation spectrum model, and compared it with the fractional Maxwell model. We applied the log-normal relaxation spectrum model to

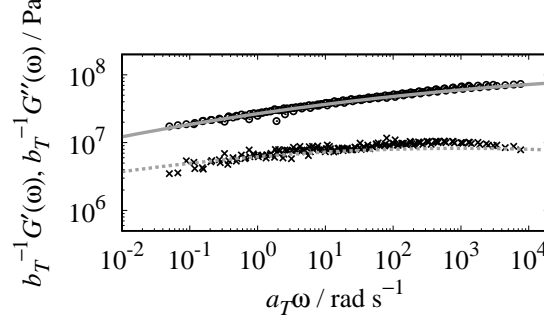


Figure 7: Storage and loss moduli of an HDPE solid at the reference temperature  $T_{\text{ref}} = 100^\circ\text{C}$  (circles and crosses) and the log-normal relaxation spectrum model (solid and dotted curves). The parameters for the log-normal relaxation spectrum model are  $G_0 = 1.2 \times 10^8 \text{ Pa}$ ,  $\tau_0 = 1.0 \times 10^{-3} \text{ s}$ , and  $s = 9.0$ .

analyze the experimental data of an HDPE both at melt and solid states, and showed that the log-normal relaxation spectrum model can reasonably explain the linear viscoelasticity data. Information geometry and information theory are currently widely used in the field of data science, but not in the field of rheology. We expect that information-theoretical analyses will provide some new aspects of rheology.

## ACKNOWLEDGMENT

The author thanks Prof. Ryuichi Tarumi (Osaka University) and Dr. Frank Nielsen (Sony Computer Science Laboratories) for giving an opportunity to study information geometry. This work was supported by Grant-in-Aid (KAKENHI) for Scientific Research Grant B No. JP23H01142.

## APPENDIX

### A Experimental

#### A.1 Materials and Methods

A high-density polyethylene (HDPE, Sigma-Aldrich, 547999) is used as received. A controlled-stress rheometer (discovery hybrid rheometer, DHR-2, TA Instruments) is used to measure the storage and loss moduli of HDPE at various temperatures, both at melt and solid states.

For high temperature measurements above the melting point, a parallel-plate fixture with a diameter 25 mm is used and the gap size is set to 1 mm. Oscillatory strains with a strain amplitude 1% is applied to the sample and the storage and loss moduli,  $G'$  and  $G''$ , are measured. The angular frequency range is  $0.05 \text{ rad/s} \leq \omega \leq 200 \text{ rad/s}$ , and the measurement temperatures are  $T = 140, 160, 180$ , and  $200^\circ\text{C}$ .

For low temperature measurements below the melting point, a parallel-plate fixture with a diameter 8 mm is used. The molten sample is loaded between the plates and the gap size is set to 1 mm. The sample was equilibrated at  $140^\circ\text{C}$  (above the melting temperature) and then cooled to  $100^\circ\text{C}$  (below the melting temperature) by  $0.5\text{K/min}$ . During the solidification, the density of the sample changes largely and it is impossible to keep the initial gap size. Therefore, the axial force for the plate is controlled to be 0 N while the temperature change, and the gap is allowed to

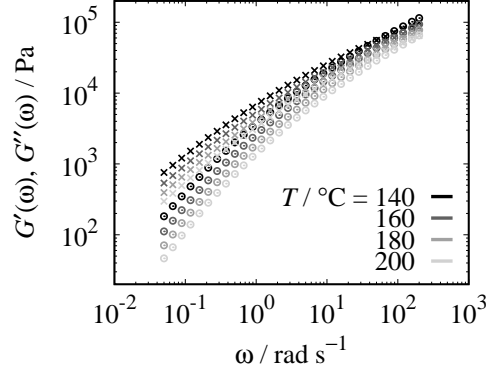


Figure 8: Storage and loss moduli of an HDPE melt at  $T = 140, 160, 180$ , and  $200^\circ\text{C}$ . Circles and crosses represent storage and loss moduli data, respectively.

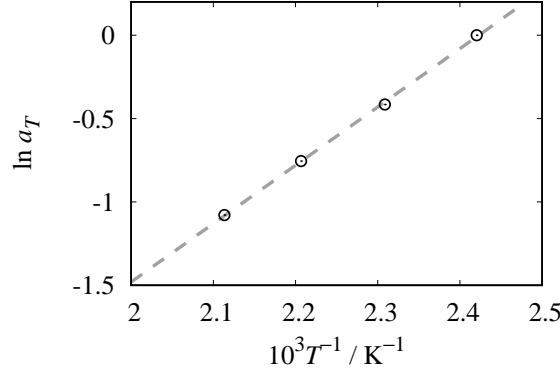


Figure 9: The Arrhenius plot for the horizontal shift factor  $a_T$  of an HDPE melt. The reference temperature is  $T_{\text{ref}} = 140^\circ\text{C}$ . Symbols show the experimental data and the dashed line shows the fitting result to the Arrhenius form.

change freely. When the temperature of the sample becomes the measurement temperature and the sample is sufficiently relaxed, the applied axial force is changed to 10N (which corresponds to the normal stress  $4.0 \times 10^5 \text{Pa}$ ) in order to prevent delamination and slippage, and the storage and loss moduli,  $G'$  and  $G''$  are measured. To improve the accuracy, oscillatory stresses are applied to the sample, instead of the oscillatory strains. The creep compliance  $J'$  and  $J''$  are measured and then converted to  $G'$  and  $G''$ . We set the stress amplitude as  $9.9 \times 10^3 \text{Pa}$ . The angular frequency range is  $0.05 \text{ rad/s} \leq \omega \leq 200 \text{ rad/s}$ , and the measurement temperatures are  $T = 100, 90, 80, 70$ , and  $60^\circ\text{C}$ . (The axial force is controlled to be 0 N when the temperature is changed.)

## A.2 Results

Fig. 8 shows the storage and loss moduli of an HDPE melt at several different temperatures. Although the clear plateau is not observed, judging from the relaxation time, HDPE is well-entangled. The relaxation time distribution seems to be very broad. By using the time-temperature superposition, we construct the master curves for  $G'(\omega)$  and  $G''(\omega)$ . We perform only the horizontal shift by the horizontal shift factor  $a_T$ , and do not perform the vertical shift. (The vertical shift factor is simply set as  $b_T = 1$  for all the temperatures.) We set the reference temperature as

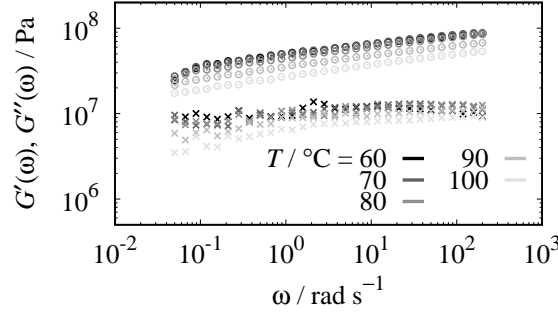


Figure 10: Storage and loss moduli of an HDPE melt at  $T = 60, 70, 80, 90,$  and  $100^\circ\text{C}$ . Circles and crosses represent storage and loss moduli data, respectively.

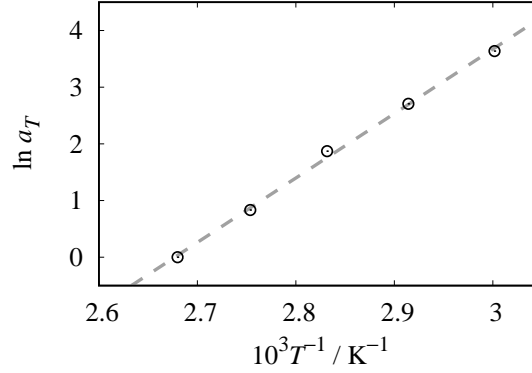


Figure 11: The Arrhenius plot for the horizontal shift factor  $a_T$  of an HDPE solid. The reference temperature is  $T_{\text{ref}} = 100^\circ\text{C}$ . Symbols show the experimental data and the dashed line shows the fitting result to the Arrhenius form.

$T_{\text{ref}} = 140^\circ\text{C}$ . The storage and loss moduli data obtained by the time-temperature superposition are shown in Fig. 6. The horizontal shift factor can be fitted to the Arrhenius form:  $\ln a_T = (E_a/R)(1/T - 1/T_{\text{ref}})$  where  $E_a$  is the activation energy and  $R$  is the gas constant. Fig. 9 shows the Arrhenius plot for the horizontal shift factor. The activation energy is estimated as  $E_a = 2.9 \times 10^1 \text{ kJ/mol}$ . This value is comparable to typical activation energies of polyethylene melts[28, 29].

Fig. 8 shows the storage and loss moduli of an HDPE solid at several different temperatures. We observe that both  $G'(\omega)$  and  $G''(\omega)$  depend on the angular frequency weakly. Such weak angular frequency dependence can be attributed to a very broad relaxation time distribution. The experimental data are scattered due to high modulus of the sample and thus not that accurate. We attempt to construct the master curves by using the time-temperature superposition. Unlike the case of the melt, we utilize both the horizontal and vertical shift factors  $a_T$  and  $b_T$ . (Note that the shift factors  $a_T$  and  $b_T$  are different from those at the melt state, because the phase structures and elementary relaxation processes of melt and solid samples are totally different.) By tuning  $a_T$  and  $b_T$ , we can construct the master curve shown in Fig. 7. Fig. 11 shows the Arrhenius plot for the horizontal shift factor  $a_T$ . The horizontal shift factor can be fitted to the Arrhenius form again, and the activation energy is estimated as  $E_a = 9.5 \times 10^1 \text{ kJ/mol}$ . This value is comparable

to typical activation energies of the crystalline relaxation process (so-called the  $\alpha$  relaxation) of polyethylene solids[30].

## References

- [1] Ferry JD, “*Viscoelastic Properties of Polymers*”, 3rd ed, (1980), Wiley, New York.
- [2] Song J, Holten-Andersen N, McKinley GH, *Soft Matter*, **19**, 7885 (2023).
- [3] Baumgaertel M, Schausberger A, Winter HH, *Rheol Acta*, **29**, 400 (1990).
- [4] Amari S, “*Information Geometry and Its Applications*”, (2016), Springer, Tokyo.
- [5] Nielsen F, *Entropy*, **22**, 1100 (2020).
- [6] Mainardi F, “*Fractional Calculus and Waves in Linear Viscoelasticity*”, (2010), Imperial College Press, London.
- [7] van Kampen NG, “*Stochastic Processes in Physics and Chemistry*”, 3rd ed, (2007), Elsevier, Amsterdam.
- [8] Evans DJ, Morriss GP, “*Statistical Mechanics of Nonequilibrium Liquids*”, 2nd ed, (2008), Cambridge University Press, Cambridge.
- [9] Beck C, Cohen EGD, *Physica A*, **322**, 267 (2003).
- [10] Frieden BR, “*Science from Fisher Information: A Unification*”, (2004), Cambridge University Press, Cambridge.
- [11] Dirac PAM, “*General Theory of Relativity*”, (1975), Wiley, New York.
- [12] Shannon CE, Weaver W, “*The Mathematical Theory of Communication*”, (1964), The University of Illinois Press, Urbana.
- [13] Fulchiron R, Michel A, Verney V, Roustant JC, *Polym Eng Sci*, **35**, 513 (1995).
- [14] Grindy SC, Learsch R, Mozhdzhi D, Cheng J, Barrett DG, Guan Z, Messersmith PB, Holten-Andersen N, *Nat Mater*, **14**, 1210 (2015).
- [15] Drozdov AD, deClaville Christiansen J, *RSC Adv*, **11**, 16860 (2021).
- [16] Takahashi H, Mori M, *Publ RIMS*, **9**, 721 (1974).
- [17] Ooura T. DE-Quadrature software package. <http://www.kurims.kyoto-u.ac.jp/~ooura/intde.html>.
- [18] Urakawa O, Nobukawa S, Inoue T, *Nihon Reoroji Gakkaishi*, **51**, 9 (2023).
- [19] Cole KS, Cole RH, *J Chem Phys*, **9**, 341 (1941).
- [20] Hilfer R, *Phys Rev E*, **65**, 061510 (2002).
- [21] Winter HH, Chambon F, *J Rheol*, **30**, 367 (1986).
- [22] Kawasaki Y, Watanabe H, Uneyama T, *Nihon Reoroji Gakkaishi*, **39**, 127 (2011).
- [23] Mainardi F, *Discrete Contin Dyn Syst B*, **19**, 2267 (2014).
- [24] Olver FWJ, Lozier DW, Boisvert RF, Clark CW (Eds), “*NIST Handbook of Mathematical Functions*”, (2010), Cambridge University Press, New York.
- [25] Viet TQ. <https://github.com/tranqv/Mittag-Leffler-function-and-its-derivative>.

- [26] Carpinteri A, Mainardi F (Eds), *“Fractals and Fractional Calculus in Continuum Mechanics”*, (1997), Springer, New York.
- [27] Li S, Petzold A, Ranga A, Yu Q, van Niekerk M, Thurn-Albrecht T, Men Y, *Macromolecules*, **58**, 5535 (2025).
- [28] Stadler FJ, Kashta J, Münstedt H, *Macromolecules*, **41**, 1328 (2008).
- [29] Kida T, Doi Y, Tanaka R, Uneyama T, Shiono T, Masubuchi Y, *Rheol Acta*, **60**(9), 511 (2021).
- [30] Strobl G, *“The Physics of Polymers”*, 2nd ed, (1997), Springer, Berlin.